Figure 1.

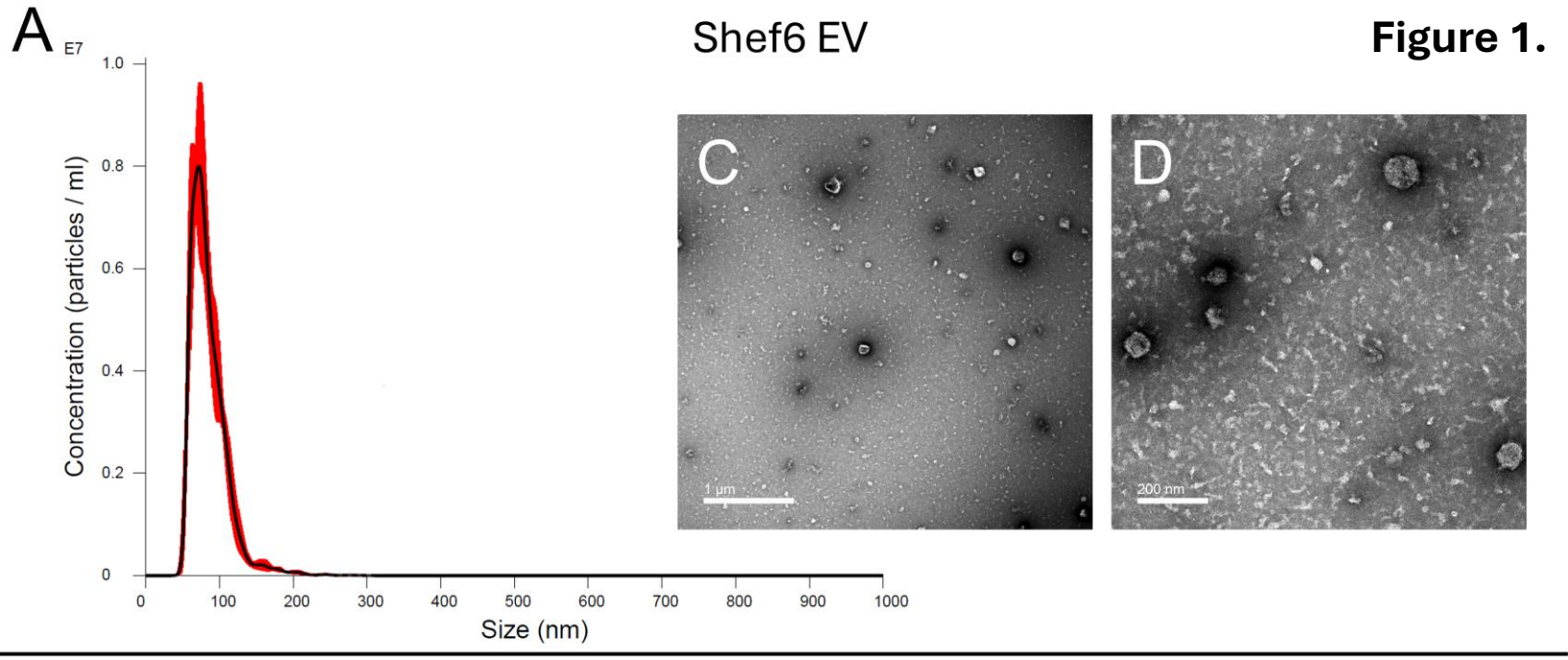
A
Shef6 EV
E7
Concentration (particles / ml)
Size (nm)
C
1 µm
D
200 nm

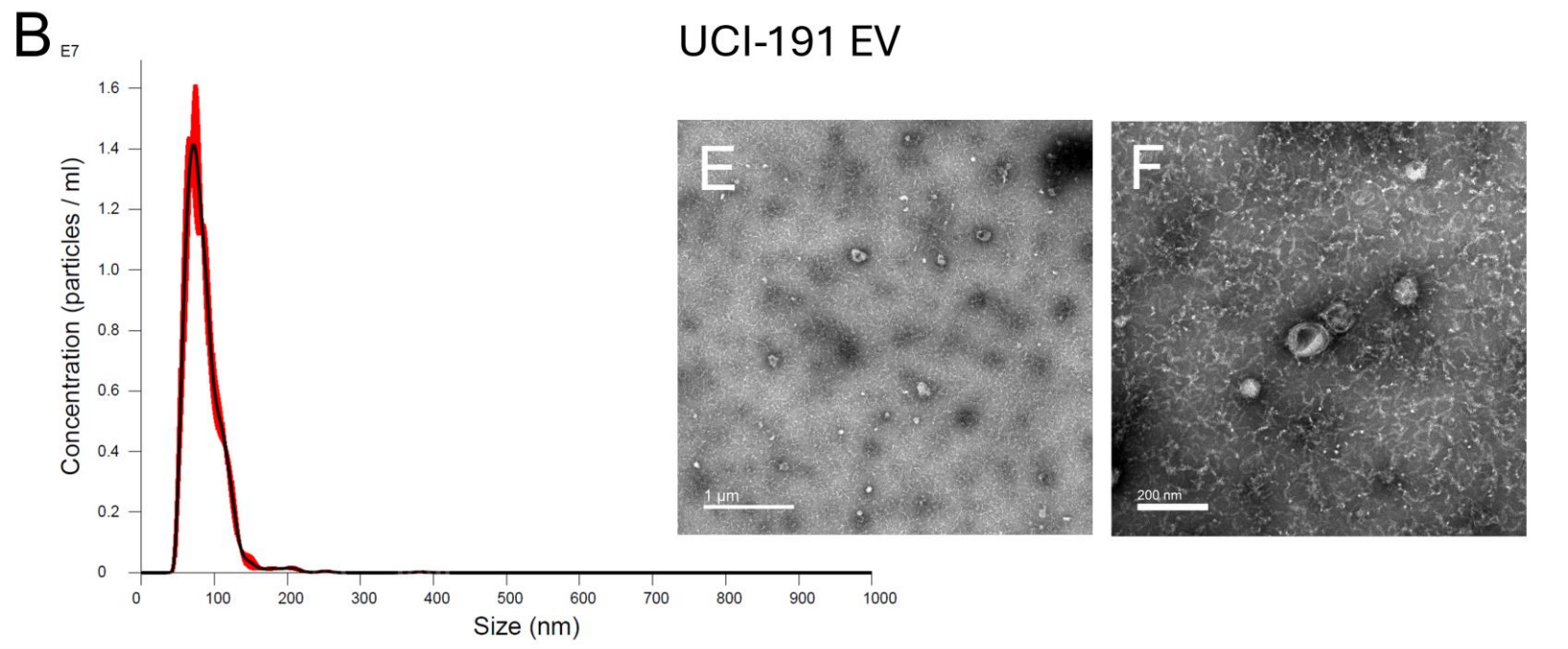
B
UCI-191 EV
E7
Concentration (particles / ml)
Size (nm)
E
1 µm
F
200 nm

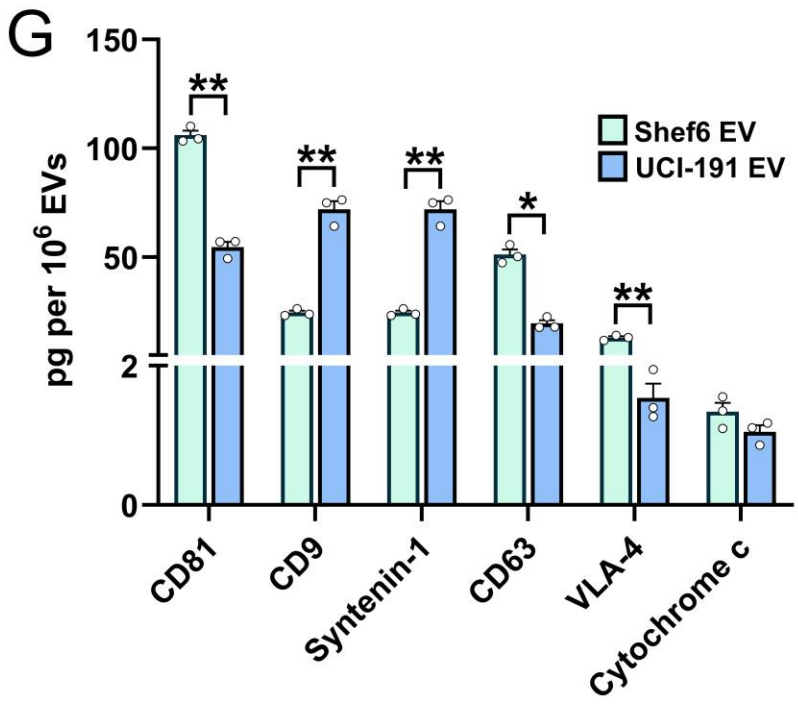
G
pg per 10^6 EVs
Shef6 EV
UCI-191 EV
CD81
CD9
Syntenin-1
CD63
VLA-4
Cytochrome c

Figure 1.

hNSC-EV characterization by size and protein markers.

Nano-particles isolated from hNSC conditioned media were characterized for size and protein marker content. **(A-B)** Particle size distribution graph for EV samples (in triplicate) characterized using a laser nanoparticle analyzer (NanoSight 3000).

Representative transmission electron micrographs of Shef6-derived (**C-D**) and UCI191-derived (**E-F**) EVs are shown. TEM magnifications were 10,000× (**B** and **E**) and 40,000× (**C** and **F**).

(G) EVs (in triplicate) were isolated, lysed, and protein content was confirmed using the ProcartaPlex™ Human Exosome Characterization Panel.

Scale bars, 1 μm (**B** and **E**) and 200 nm (**C** and **F**).

Figure 2.

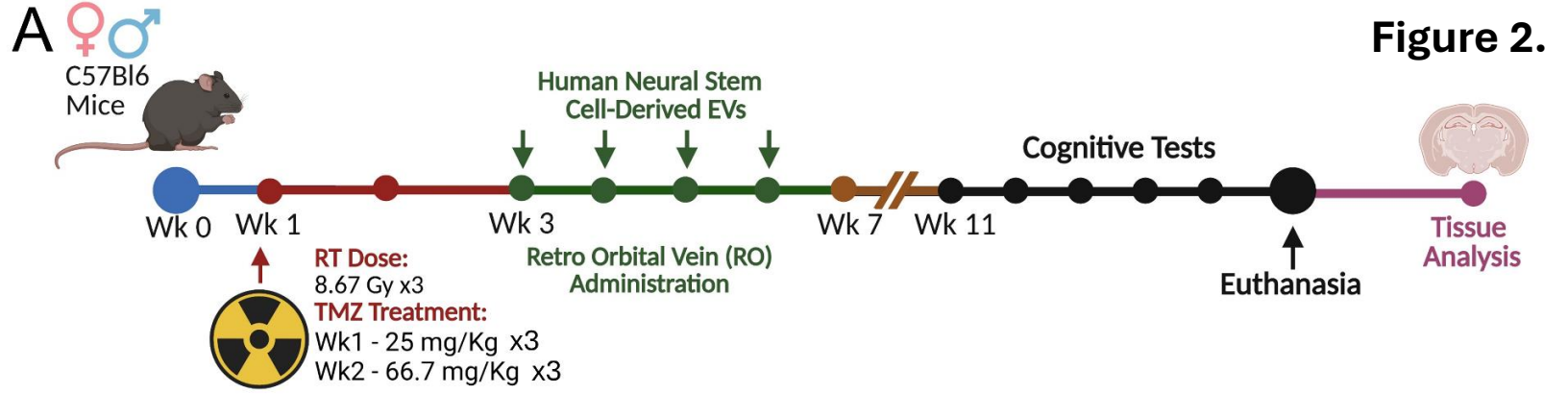

♂ Males ♀ Females

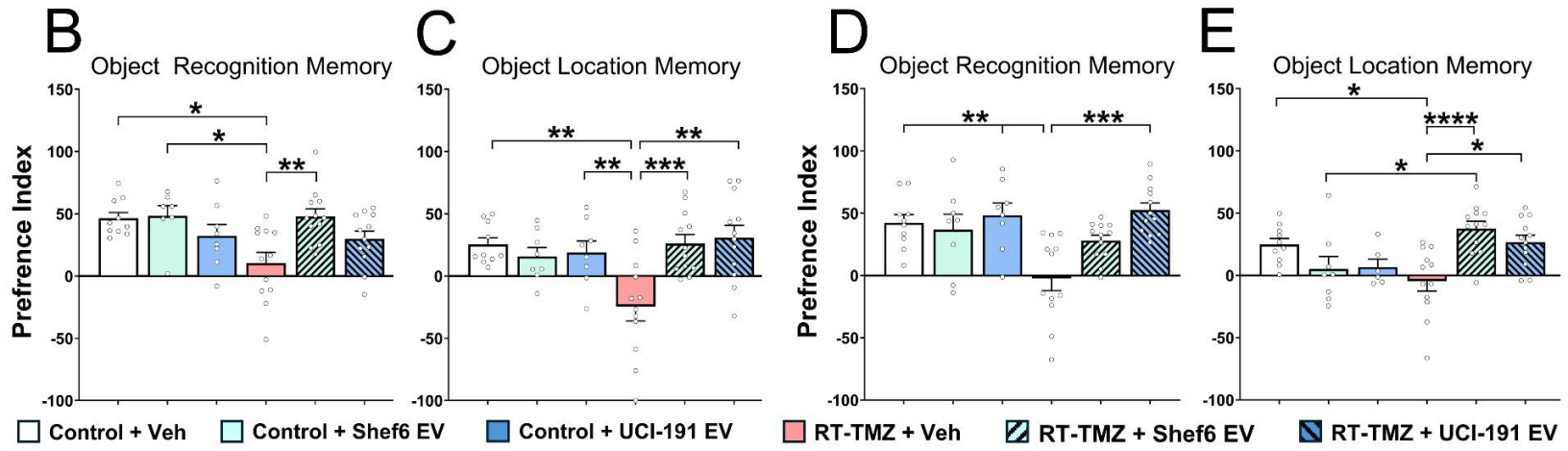

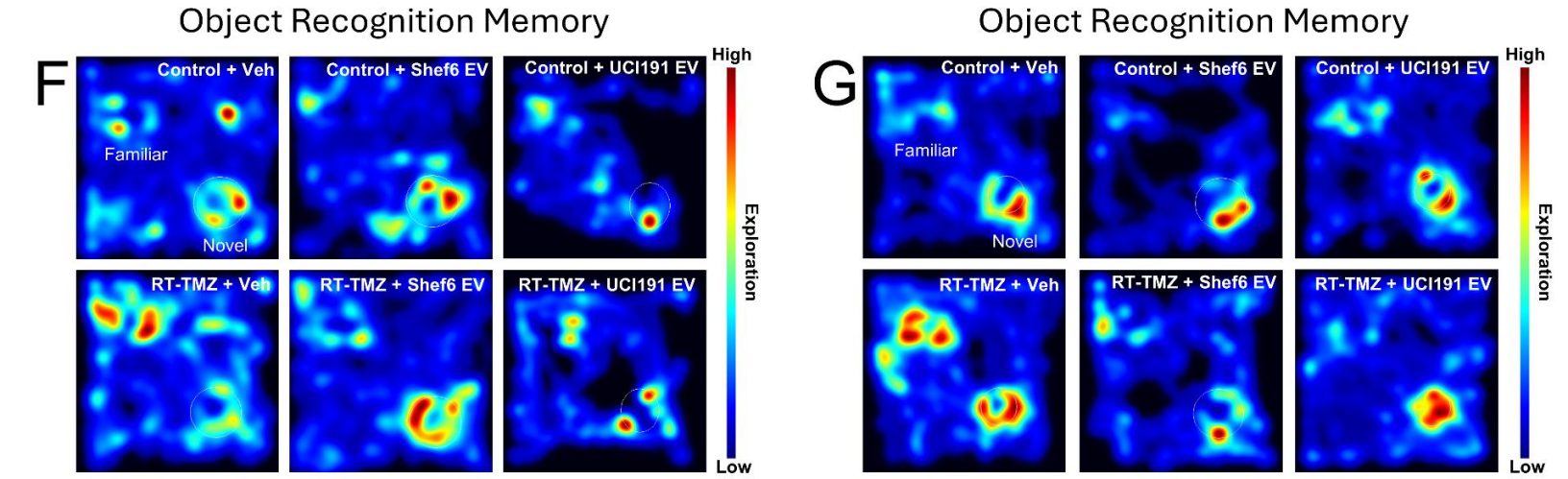

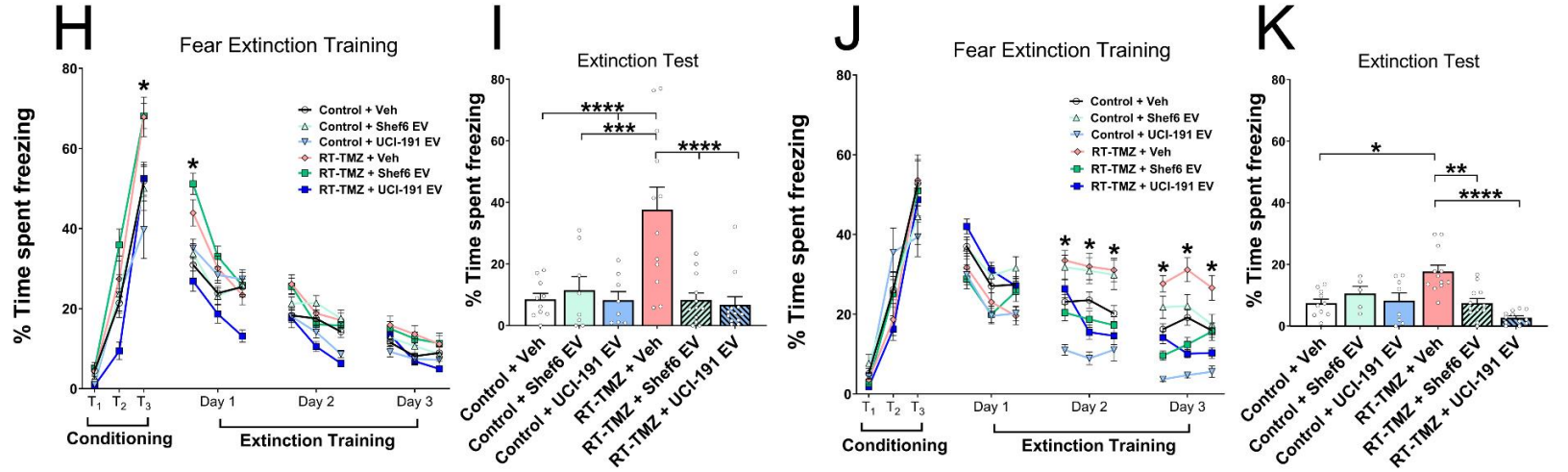

Figure 2.

hNSC-EVs prevent cognitive impairments following combined cranial irradiation therapy and chemotherapy.

(A) Research design: Four-month-old WT (C57Bl6) male and female mice received fractionated cranial radiation therapy (8.67 Gy ×3, every other day), concomitant TMZ (25 mg/kg ×3, IP) 24h after each RT, and adjuvant TMZ (66.7 mg/kg ×3, IP) 72h after the concomitant TMZ, every other day, over the course of two weeks. 72 h after completion of RT-TMZ treatment, mice received bilateral retro-orbital vein (RO) injections of hNSC-EVs (RT-TMZ + Shef6 EV; RT-TMZ + UCI191 EV) or sham RO injections (RT-TMZ + Veh; sterile PBS) once weekly for 4-weeks. Four weeks after the final EV treatment, cognitive and behavioral tasks (ORM, OLM, FE, EPM, OFT) were administered. After completion of cognitive testing, animals were euthanized, and their brains were collected for cellular and molecular analyses (See **Suppl. Fig. S1** for OFT and EPM data; **A,** designed using *BioRender*).

(B-E) Spontaneous exploration tasks, ORM, and OLM for male and female mice. Cognitive performance data are reported as Preference Index (PI), calculated by $[(T_{Novel}/ T_{Total})-(T_{Familiar}/ T_{Total})] \times 100$, where T is the time (s) exploring novel or familiar object (or location), and the total time exploring both.

(F-G) Representative heatmaps depicting animal exploration of familiar or novel objects throughout the ORM testing arena (See **Suppl. Fig. S2** for OLM heatmaps).

(H-K) Graphical depiction of sequential fear extinction (Days 1-3) in male **(H)** and female **(J)** mice after the initial fear conditioning phase (T_{1-3}). Successful extinction of the conditioned fear response is evidenced by a decrease in the percentage of time spent freezing (**H** and **J**). Analysis of the percentage of time spent freezing on the final Test Day of FE (**I** and **K**).

Data are represented by mean ± SEM (N = 5-12 animals/group). P-values were calculated by two-way ANOVA and Bonferroni's multiple comparisons test. *, $P \leq 0.05$; **, $P \leq 0.01$; *** $P \leq 0.001$; ****, $P \leq 0.0001$.

Figure 3.

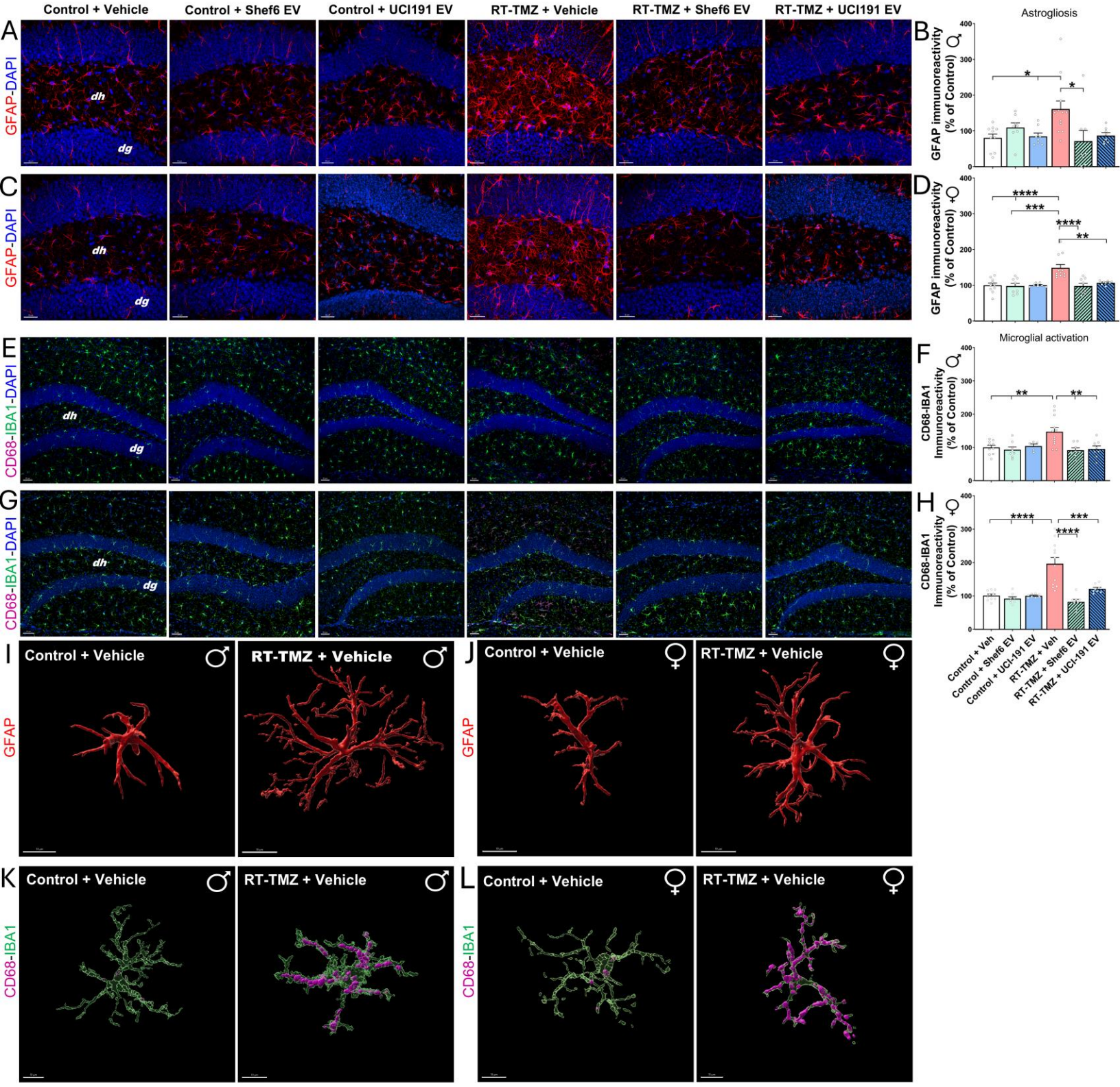
Control + Vehicle
Control + Shef6 EV
Control + UCI191 EV
RT-TMZ + Vehicle
RT-TMZ + Shef6 EV
RT-TMZ + UCI191 EV
A
GFAP-DAPI
dh
dg
B
Astrogliosis
GFAP immunoreactivity (% of Control)
C
D
E
CD68-IBA1-DAPI
F
Microglial activation
CD68-IBA1 Immunoreactivity (% of Control)
G
H
Control + Veh
I
GFAP
J
K
CD68-IBA1
L

Figure 3.

hNSC-EVs prevent neuroinflammation following combined cranial radiation and chemotherapy.

(A-D) Confocal fluorescent micrographs and volumetric analysis of astrogliosis in male and female mice. Immunofluorescence staining, confocal microscopy, and 3D algorithm-based quantification for the astrocytic cytoskeleton glial fibrillary acidic protein (GFAP; red) with DAPI nuclear counter stain (blue) in the hippocampal dentate hilus (*dh*) and dentate gyrus (*dg*).

(E-H) Dual labeled confocal fluorescent micrographs and volumetric quantification of IBA1 and CD68 colocalization to quantify microglial activation in male and female mice. Immunofluorescence staining, confocal microscopy, and 3D algorithm-based quantification for a pan microglial marker (IBA1, green), and lysosomal membrane marker CD68 (magenta) with DAPI nuclear counter stain (blue) in the hippocampal dentate hilus (*dh*) and dentate gyrus (*dg*).

High resolution immunoreactive surface rendering of single cell images in the Control + Veh and RT-TMZ + Veh groups in male and female brains for $GFAP^+$ astrocytes (**I** and **J**) and IBA1-CD68+ dual-labeled microglia (**K** and **L**).

dh, dentate hilus, and *dg, dentate gyrus*. Confocal z stacks were acquired at 40× (**A** and **C**, 1.30 numerical aperture) and 20× (**E** and **G**, 0.75 numerical aperture) magnifications. Scale bars, 30 μm (**A** and **C**), 50 μm (**E** and **G**), and 10 μm (**I** and **J**).

Data are represented by mean ± SEM (N = 5-12 animals/group). *P* values were calculated by one-way ANOVA and Tukey's multiple comparisons tests. *, $P \leq 0.05$; **, $P \leq 0.01$; *** $P \leq 0.001$; ****, $P \leq 0.0001$.

Figure 4.

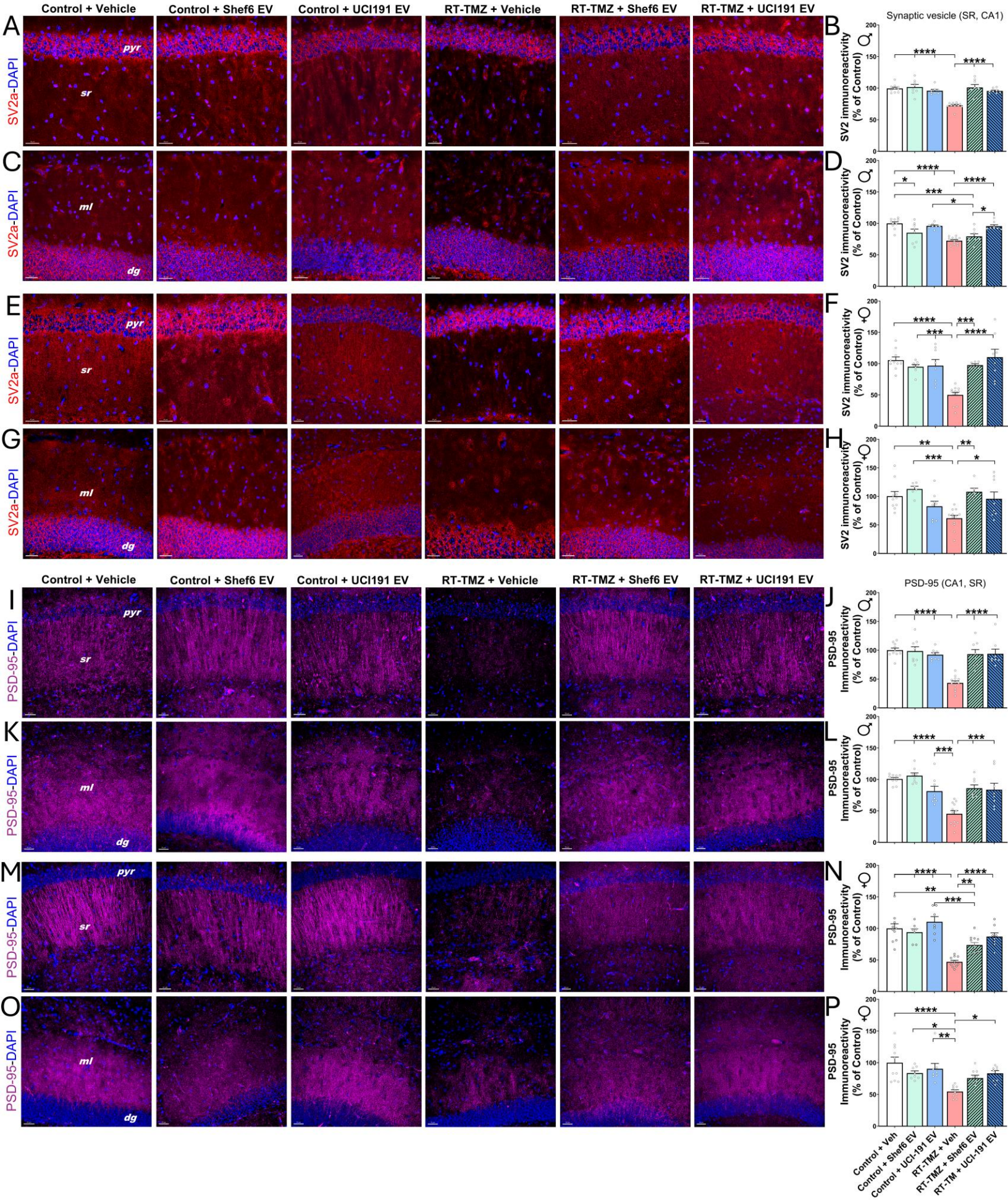
Control + Vehicle
Control + Shef6 EV
Control + UCI191 EV
RT-TMZ + Vehicle
RT-TMZ + Shef6 EV
RT-TMZ + UCI191 EV
A
B
C
D
E
F
G
H
I
J
K
L
M
N
O
P
SV2a-DAPI
PSD-95-DAPI
pyr
sr
ml
dg
Synaptic vesicle (SR, CA1)
PSD-95 (CA1, SR)
SV2 immunoreactivity (% of Control)
PSD-95 Immunoreactivity (% of Control)
♂
♀
Control + Veh
Control + Shef6 EV
Control + UCI-191 EV
RT-TMZ + Veh
RT-TMZ + Shef6 EV
RT-TM + UCI-191 EV

Figure 4.

hNSC-EVs prevent synaptic density loss following combined cranial radiation therapy and chemotherapy.

Fluorescent confocal micrographs and volumetric quantification of synaptic density in male (**A**-**D**) and female (**E**-**H**) mice.

Immunofluorescence staining, confocal microscopy, and 3D algorithm-based quantification for synaptic vesicle glycoprotein 2A (SV2a; red) with DAPI nuclear counter stain (blue) in the hippocampal CA1 pyramidal cell layer (*pyr*) and stratum radiation (*sr*) (**A** and **E**), and the molecular layer (*ml*) and dentate gyrus (*dg*) (**C** and **G**).

Representative confocal micrographs and analysis of postsynaptic density protein, PSD-95 (magenta) with DAPI nuclear counter staining in male (**I**-**L**) and female (**M**-**P**) hippocampal *pyr* and *sr subregions* of CA1 (**I and M**), and the *ml* and *dg* (**K and O**). Scale bars, 30 μm (**A**-**O**).

Data are represented by mean ± SEM (N = 6-12 animals/group). *P* values were calculated by repeated measures ANOVA and Tukey's multiple comparisons tests. *, $P \leq 0.05$; **, $P \leq 0.01$; *** $P \leq 0.001$; ****, $P \leq 0.0001$.

Figure 5.

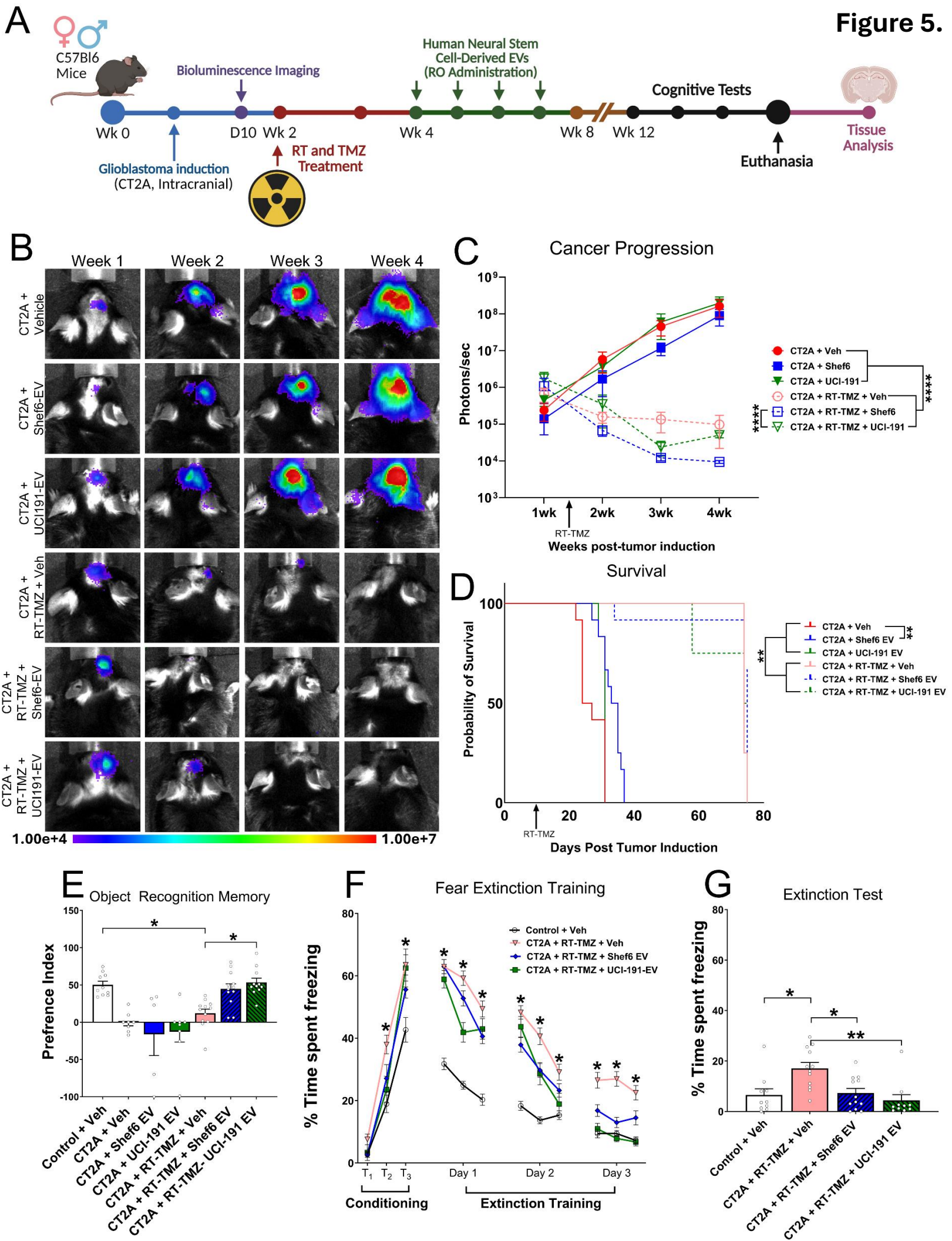
A
C57Bl6 Mice
Bioluminescence Imaging
Human Neural Stem Cell-Derived EVs (RO Administration)
Cognitive Tests
Wk 0
D10
Wk 2
Wk 4
Wk 8
Wk 12
Tissue Analysis
Glioblastoma induction (CT2A, Intracranial)
RT and TMZ Treatment
Euthanasia
B
Week 1
Week 2
Week 3
Week 4
CT2A + Vehicle
CT2A + Shef6-EV
CT2A + UCI191-EV
CT2A + RT-TMZ + Veh
CT2A + RT-TMZ + Shef6-EV
CT2A + RT-TMZ + UCI191-EV
1.00e+4
1.00e+7
C
Cancer Progression
Photons/sec
1wk
2wk
3wk
4wk
RT-TMZ
Weeks post-tumor induction
CT2A + Veh
CT2A + Shef6
CT2A + UCI-191
CT2A + RT-TMZ + Veh
CT2A + RT-TMZ + Shef6
CT2A + RT-TMZ + UCI-191
****
****
D
Survival
Probability of Survival
RT-TMZ
Days Post Tumor Induction
CT2A + Veh
CT2A + Shef6 EV
CT2A + UCI-191 EV
CT2A + RT-TMZ + Veh
CT2A + RT-TMZ + Shef6 EV
CT2A + RT-TMZ + UCI-191 EV
**
**
E
Object Recognition Memory
Prefrence Index
Control + Veh
CT2A + Veh
CT2A + Shef6 EV
CT2A + UCI-191 EV
CT2A + RT-TMZ + Veh
CT2A + RT-TMZ + Shef6 EV
CT2A + RT-TMZ- UCI-191 EV
F
Fear Extinction Training
% Time spent freezing
Control + Veh
CT2A + RT-TMZ + Veh
CT2A + RT-TMZ + Shef6 EV
CT2A + RT-TMZ + UCI-191-EV
T1
T2
T3
Day 1
Day 2
Day 3
Conditioning
Extinction Training
G
Extinction Test
% Time spent freezing
Control + Veh
CT2A + RT-TMZ + Veh
CT2A + RT-TMZ + Shef6 EV
CT2A + RT-TMZ + UCI-191 EV

Figure 5.

hNSC-EVs improve cognitive function in brain cancer-bearing mice without interfering with the therapeutic efficacy of combined cranial radiation therapy and chemotherapy.

(A) Research design: Four-month-old male and female C57Bl6 WT mice were induced with glioblastoma using stereotaxic-guided intracranial injections of murine CT2A-luc cells. Cancer burden was confirmed ten days post induction and monitored over the course of the study through bioluminescence imaging and quantified by the IVIS® Spectrum module. After confirmation of tumor development, animals were treated with combined cranial radiation therapy and chemotherapy as described in **Fig. 1** (CT2A+ RT-TMZ + Veh). Mice were then treated with hNSC-EVs (CT2A + RT-TMZ + Shef6 EV, CT2A + RT-TMZ + UCI191 EV), followed by cognitive and behavioral testing (ORM, FE, EPM, OFT). After completion of cognitive testing, mice were euthanized, and tissues were collected (designed using *BioRender.com*). See **Suppl. Fig. S3** for OFT and EPM data.

(B) Representative BLI depicting progression of glioma over four weeks post-tumor induction.

(C) Tumor growth and progression as measured by the relative bioluminescence and presented logarithmically.

(D) Kaplan-Meier survival plot of cancer-bearing animals receiving vehicle, EV or RT-TMZ treatments.

(E) The object recognition memory (ORM) task presented as Preference Index, calculated by: by $[(T_{Novel}/ T_{Total})-(T_{Familiar}/ T_{Total})] \times 100$, where T is the time (s) exploring novel or familiar object (or location), and the total time exploring both. See **Suppl. Table T1** for complete list of statistical significance showing P values. See **Suppl. Fig. S4** for ORM heatmap.

(F) Fear extinction training: Graphical representation of sequential fear extinction phase (Days 1-3) after initial fear conditioning (T_{1-3}). Successful extinction training is observed as a decrease in percentage of time spent freezing by Day 3.

(G) Extinction test: Quantification of percentage of time spent freezing on final Test Day of fear extinction testing paradigm.

Data are represented by mean ± SEM. N = 4-12 animals per group (each group included 2-4 females). P-values were calculated by repeated measures ANOVA and Bonferroni's multiple comparisons tests (**C** and **E**) and by Lognormal Brown-Forsythe and Welch ANOVA and Dunnett's T3 multiple comparisons test (**D**). *, $P \leq 0.05$; **, $P \leq 0.01$; *** $P \leq 0.001$; ****, $P \leq 0.0001$.

Figure 6.

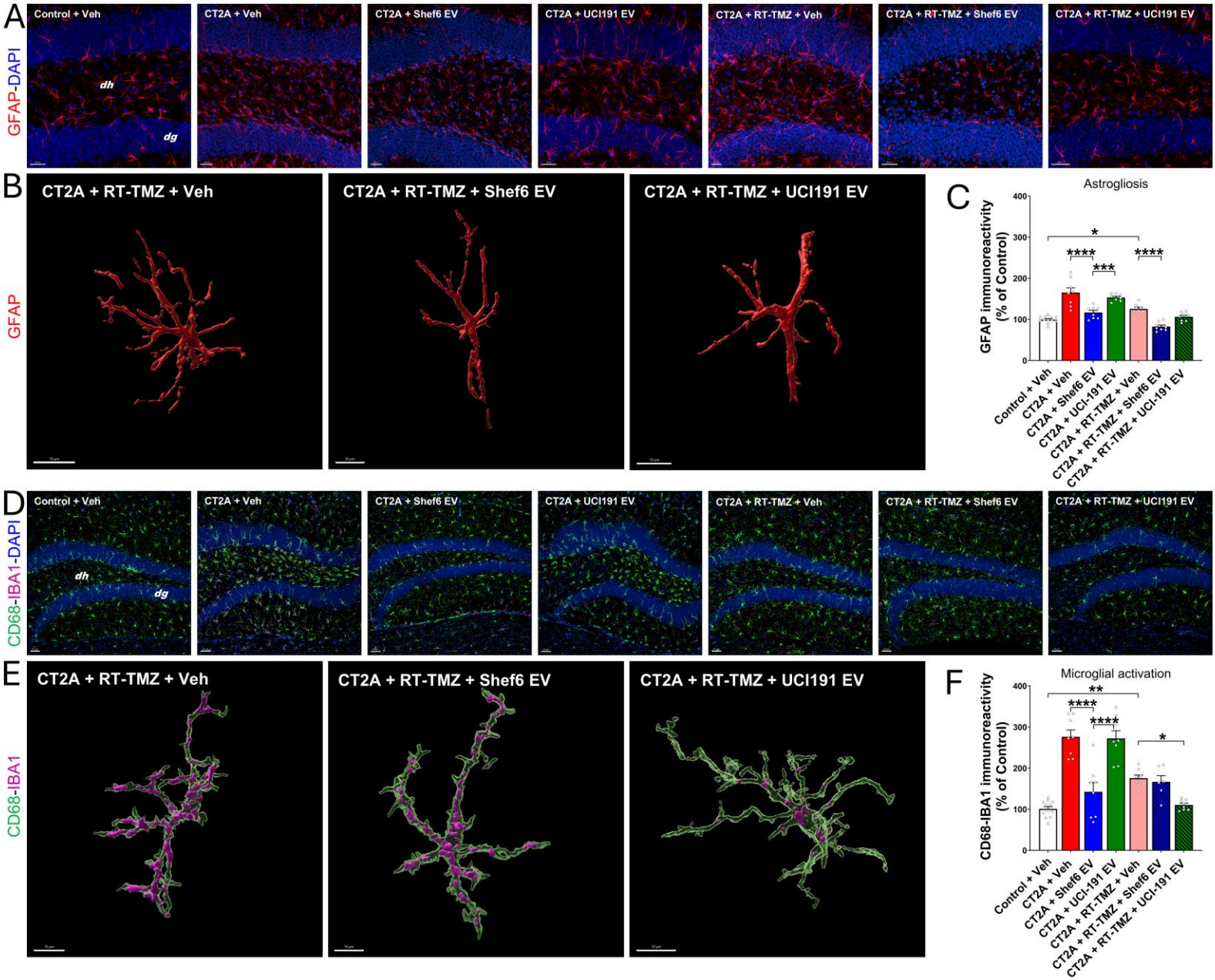
A
GFAP-DAPI
Control + Veh
CT2A + Veh
CT2A + Shef6 EV
CT2A + UCI191 EV
CT2A + RT-TMZ + Veh
CT2A + RT-TMZ + Shef6 EV
CT2A + RT-TMZ + UCI191 EV
dh
dg
B
GFAP
CT2A + RT-TMZ + Veh
CT2A + RT-TMZ + Shef6 EV
CT2A + RT-TMZ + UCI191 EV
C
Astrogliosis
GFAP immunoreactivity (% of Control)
400
300
200
100
0
*
****
***
****
Control + Veh
CT2A + Veh
CT2A + Shef6 EV
CT2A + UCI-191 EV
CT2A + RT-TMZ + Veh
CT2A + RT-TMZ + Shef6 EV
CT2A + RT-TMZ + UCI-191 EV
D
CD68-IBA1-DAPI
Control + Veh
CT2A + Veh
CT2A + Shef6 EV
CT2A + UCI191 EV
CT2A + RT-TMZ + Veh
CT2A + RT-TMZ + Shef6 EV
CT2A + RT-TMZ + UCI191 EV
dh
dg
E
CD68-IBA1
CT2A + RT-TMZ + Veh
CT2A + RT-TMZ + Shef6 EV
CT2A + RT-TMZ + UCI191 EV
F
Microglial activation
CD68-IBA1 immunoreactivity (% of Control)
400
300
200
100
0
**
****
****
*
Control + Veh
CT2A + Veh
CT2A + Shef6 EV
CT2A + UCI-191 EV
CT2A + RT-TMZ + Veh
CT2A + RT-TMZ + Shef6 EV
CT2A + RT-TMZ + UCI-191 EV

Figure 6.

hNSC-EVs reduce neuroinflammation in brain cancer-bearing mice receiving combined cranial radiation therapy and chemotherapy.

(A-B) Visual representation and quantification of astrogliosis. Immunofluorescence staining, confocal microscopy, and 3D algorithm-based quantification for GFAP (red) with a DAPI nuclear counter stain (blue) in the dentate hilus (*dh*) and dentate gyrus (*dg*) (**A** and **C**). See **Suppl. Table T2** for complete list of significant test comparisons. **(B)** High resolution reconstruction of $GFAP^+$ surface for the CT2A + RT-TMZ + Veh, CT2A + RT-TMZ + Shef6 EV, and CT2A + RT-TMZ + UCI191 EV groups.

(D-F) Visual depiction and analysis of microglial activation. CD68-IBA1 dual immunofluorescence staining with DAPI nuclear counter stain (blue) in the dentate hilus (*dh*) and dentate gyrus (*dg*). **(E)** High resolution surface rendering of CD68-IBA1 colocalization is shown for CT2A + RT-TMZ + Veh, CT2A + RT-TMZ + Shef6 EV, and CT2A + RT-TMZ + UCI191 EV groups. Confocal z stacks were acquired at 40× (**A,** 1.30 numerical aperture) and 20× (**D,** 0.75 numerical aperture) magnifications.

Scale bars, 30 μm (**A**), 10 μm (**B** and **E**), and 50 μm (**D**). Data are represented by mean ± SEM (N = 5-12 animals/group). P-values were calculated by repeated measures ANOVA and Tukey's multiple comparisons tests. *, $P \leq 0.05$; **, $P \leq 0.01$; *** $P \leq 0.001$; ****, $P \leq 0.0001$.

Figure 7.

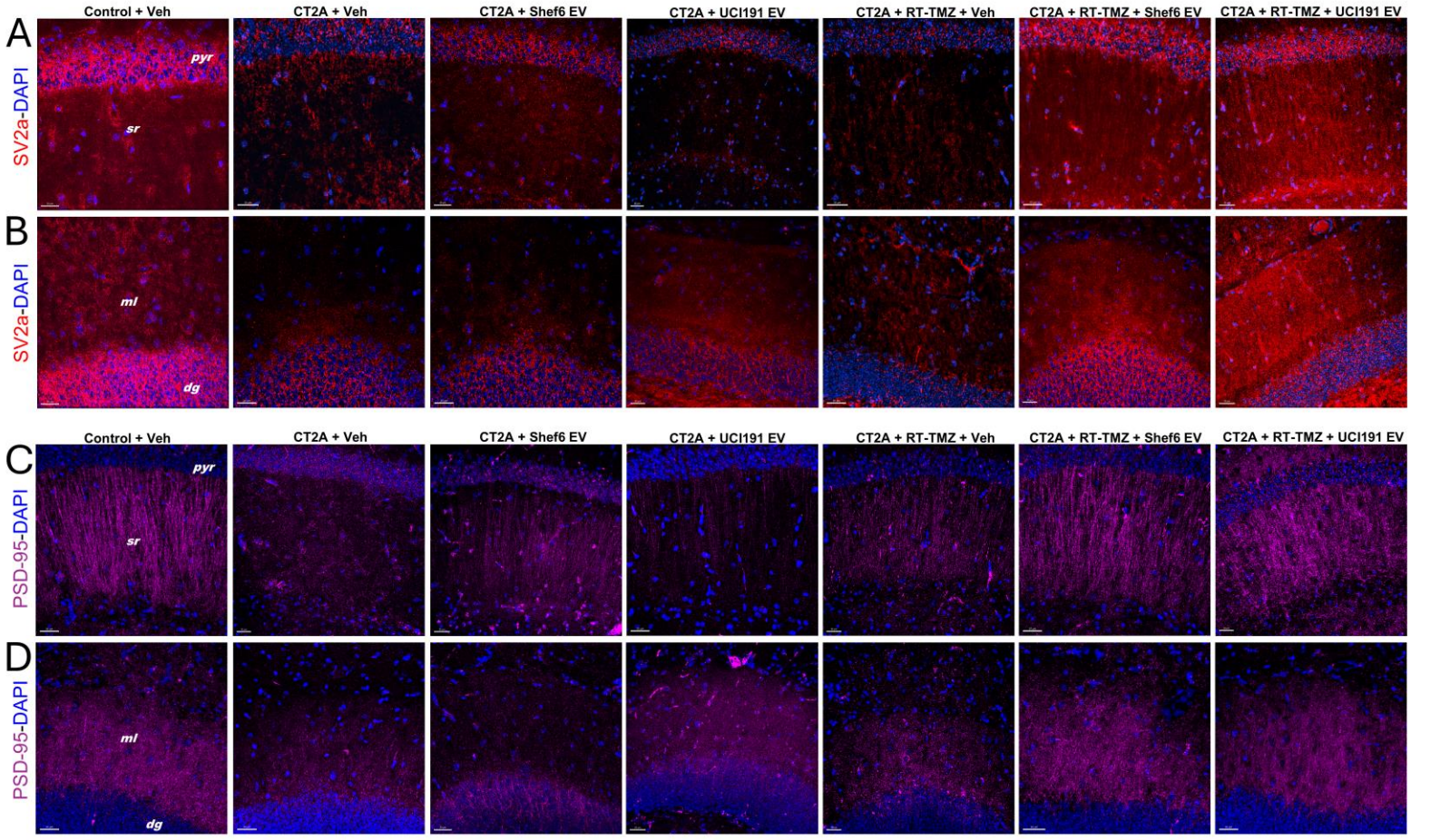
A
B
C
D
Control + Veh
CT2A + Veh
CT2A + Shef6 EV
CT2A + UCI191 EV
CT2A + RT-TMZ + Veh
CT2A + RT-TMZ + Shef6 EV
CT2A + RT-TMZ + UCI191 EV
SV2a-DAPI
PSD-95-DAPI
pyr
sr
ml
dg

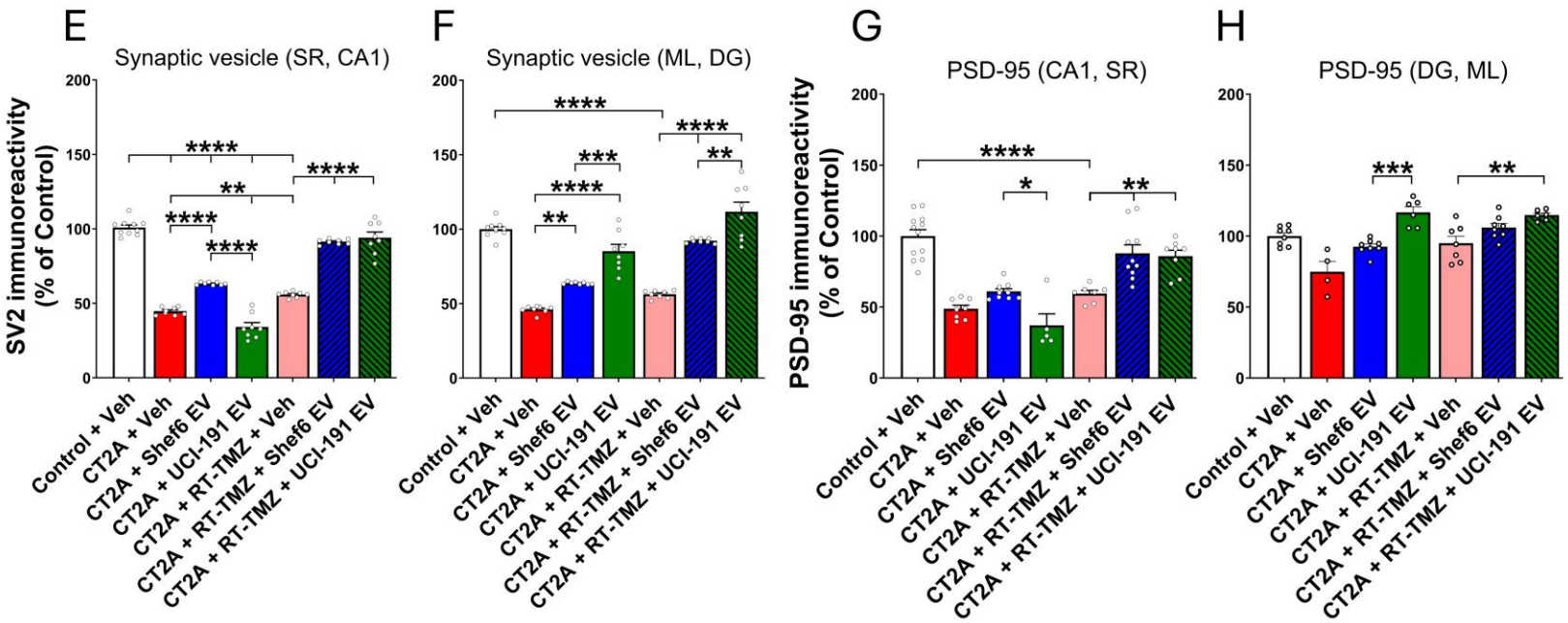
E
Synaptic vesicle (SR, CA1)
F
Synaptic vesicle (ML, DG)
G
PSD-95 (CA1, SR)
H
PSD-95 (DG, ML)
SV2 immunoreactivity (% of Control)
PSD-95 immunoreactivity (% of Control)
Control + Veh
CT2A + Veh
CT2A + Shef6 EV
CT2A + UCI-191 EV
CT2A + RT-TMZ + Veh
CT2A + RT-TMZ + Shef6 EV
CT2A + RT-TMZ + UCI-191 EV

Figure 7.

hNSC-EVs restore synaptic density in the glioma-bearing brain treated with combined irradiation and chemotherapy.

(A-B) Immunofluorescence confocal micrographs of synaptic vesicle glycoprotein 2A (SV2a; red) with DAPI nuclear counter stain (blue) in the pyramidal cell layer (*pyr*) and stratum radiatum (*sr*) of CA1 (**A**) and the molecular layer (*ml*) and dentate gyrus (*dg*) in the hippocampus (**B**).

(C-D) Fluorescent confocal micrographs of postsynaptic density protein 95 (PSD-95; magenta) with DAPI nuclear counter stain (blue) in the pyramidal cell layer (*pyr*) and stratum radiatum (*sr*) of CA1 (**C**) and the molecular layer (*ml*) and dentate gyrus (*dg*) in the hippocampus (**D**).

(E-F) Volumetric quantification of SV2a immunoreactive puncta in the CA1 *sr* **(E)** and *ml dg* **(F)** subregions. See **Suppl. Table T4 –T5** for all the group comparisons with significance.

(G-H) Volumetric quantification of PSD-95 immunoreactive puncta CA1 **(G)** and *dg* **(H)**. See **Suppl Table T6-T7** for all the group comparisons with significance.

Scale bars, 30 μm (**A**-**D**). Data are represented by mean ± SEM (N = 4-8 animals/group). P-values were calculated by repeated measures ANOVA and Tukey's multiple comparisons tests. *, $P \leq 0.05$; **, $P \leq 0.01$; *** $P \leq 0.001$; ****, $P \leq 0.0001$.

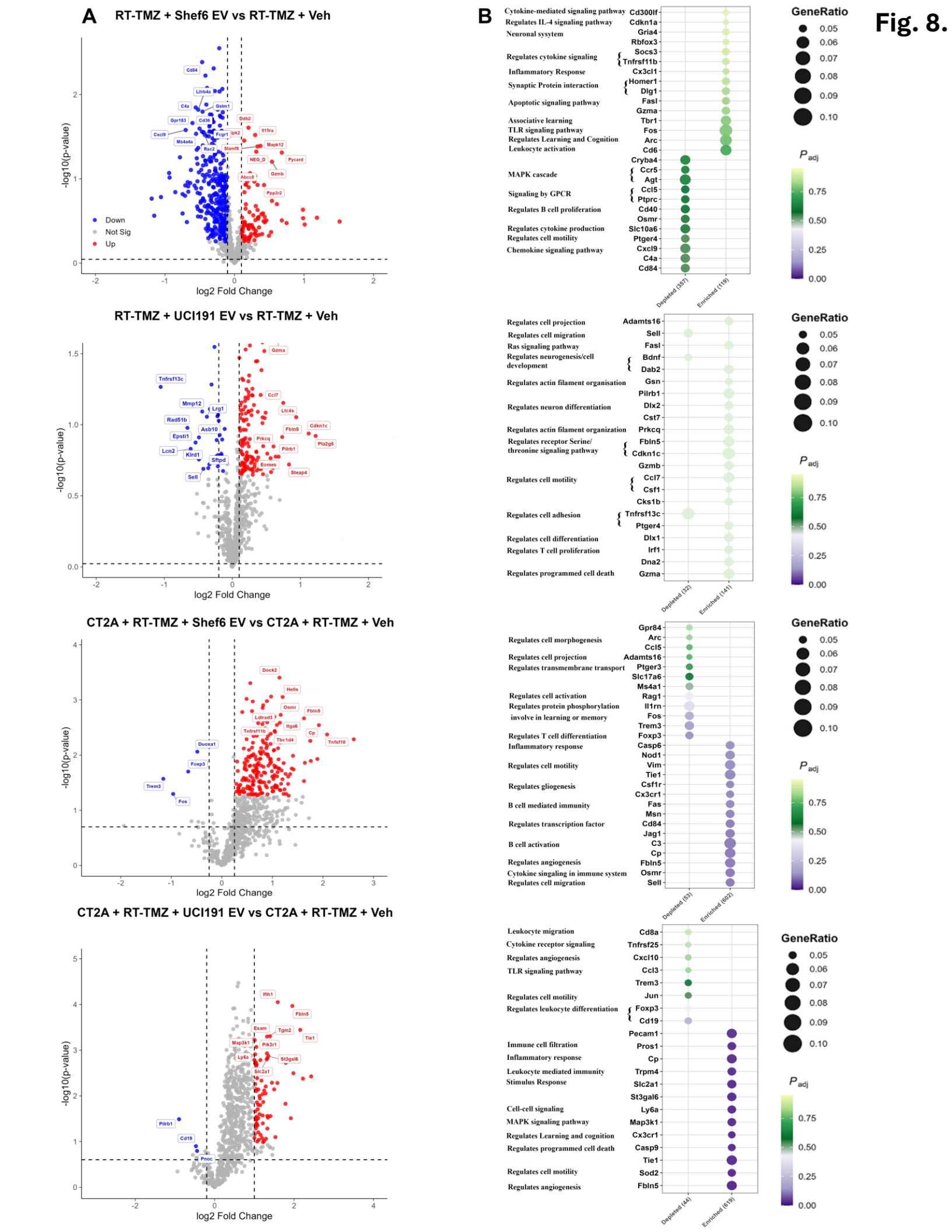
A
RT-TMZ + Shef6 EV vs RT-TMZ + Veh
RT-TMZ + UCI191 EV vs RT-TMZ + Veh
CT2A + RT-TMZ + Shef6 EV vs CT2A + RT-TMZ + Veh
CT2A + RT-TMZ + UCI191 EV vs CT2A + RT-TMZ + Veh
-log10(p-value)
log2 Fold Change
Down
Not Sig
Up
B
GeneRatio
Padj
Depleted (357)
Enriched (119)
Depleted (32)
Enriched (141)
Depleted (53)
Enriched (602)
Depleted (44)
Enriched (619)

Fig. 8.

Figure 8.

Comparative gene expression analysis of cancer and non-cancer mice brains treated with hNSC-EVs.

(A) Volcano plots depict differential gene expression across the experimental groups, including RT-TMZ + Shef6 EV (N = 3), RT-TMZ + UCI-191 EV (N = 3), CT2A + RT-TMZ + Shef6 EV (N = 3), and CT2A + RT-TMZ + UCI-191 EV (N = 3), each compared with their corresponding controls, with each point representing an individual gene. The x-axis corresponds to the log2 fold change (magnitude of expression difference between conditions), while the y-axis corresponds to the –log10 of the adjusted P value (statistical significance after multiple testing correction, Benjamini-Hochberg FDR). Downregulated genes migrate further to the left, while upregulated genes displayed further to the right. Higher $-\log_{10}$P values indicated higher statistically significant gene expression. Significance thresholds used were adjusted $P < 0.05$ and log2 fold change > 1. Red: Strongly upregulated, high significance. Blue: Strongly downregulated, high significance.

(B) Bubble plots of differentially expressed genes (DEGs) in RT-TMZ + Shef6 EV, RT-TMZ + UCI-191 EV, CT2A + RT-TMZ + Shef6 EV, and CT2A + RT-TMZ + UCI-191 EV compared with Control + Veh (N = 4). Bubble plot showing significantly enriched and depleted genes across the experimental group relative to Control. Each bubble represents an individual gene meeting the criteria $|\log_2$ fold change$| > 0.2$ and adjusted $P < 0.5$. Genes are grouped by regulation status (Enriched or Depleted) and ordered by statistical significance ($-\log_{10}$ P value). Bubble size corresponds to the scaled magnitude of differential expression (GeneRatio derived from $|\log_2$ fold change$|$), while bubble color indicates the adjusted P value, with darker colors representing higher statistical significance. Gene ontology terms displayed along the x-axis denote Metascape-derived functional enrichment pathways associated with each gene.